AFM-IN-SEM ANALYSES OF THIORPHAN ASSEMBLY ON ZNO POLAR AND NONPOLAR SURFACES

[1]Egor UKRAINTSEV, [1]Hadi HEMATIAN, [2]Jan NEUMAN, [1]Bohuslav REZEK

[1]Faculty of Electrical Engineering, Czech Technical University in Prague, Prague, Czech Republic, EU, ukraiego@fel.cvut.cz

[2]NenoVision s. r. o., Brno, Czech Republic, EU

https://doi.org/10.37904/nanocon.2023.4761

Abstract

Despite the importance of thiorphan as a small molecule with vital biological roles, its interactions with zinc oxide (ZnO) nanomaterials that are prospective in drug delivery and theranostic applications have not yet been sufficiently explored. Here the impact of surface polarity of different ZnO surfaces on thiorphan adsorption is studied experimentally by combined in-situ scanning electron microscope (SEM) and atomic force microscope (AFM). Polar ZnO surfaces cause formation of thiorphan nanodots (4 nm or 25 nm), where the size of the nanodots depends on the direction of the surface dipoles. Nonpolar ZnO surfaces cause self-assembly of thiorphan into nanoislands and nanolayers with characteristic 4 nm layer thickness. AFM-in-SEM data shows clear correlation between secondary electron intensity of molecules in SEM and their height in AFM on polar ZnO surface whereas anti-correlation is observed on nonpolar ZnO surface. The secondary electron emission from the same molecule thus depends on its orientation, structure it assembles into and it can be controlled by direction of the substrate surface dipole.

Keywords: Atomic force microscopy, scanning electron microscopy, thiorphan, ZnO surfaces, molecular assembly

1. INTRODUCTION

Correlative microscopy is a combination of two or more independent microscopy techniques applied to simultaneously study of exactly the same region of interest (ROI) under exactly the same conditions, i.e. atmosphere, pressure, humidity, temperature etc. Several common examples of correlative imaging are correlative light microscopy and scanning electron microscopy (SEM) [1,2], correlative light microscopy and atomic force microscopy (AFM) [3], correlative fluorescence and plasmonic imaging [4], correlative neutron and X-ray tomography [5].

In this work correlative probe and electron microscopy (CPEM) [6,7] is used to record AFM topography data simultaneously with SEM electron emission data. One main advantage of AFM-in-SEM technology is the possibility to use SEM data for precise navigation of AFM probe to ROI. Second, by moving AFM stage relative to SEM beam and to AFM probe correlating images are obtained simultaneously with practically constant offset between AFM and SEM images. This technique was thus applied to study the effect of thiorphan adsorption on electron emission contrast.

Thiorphan ((DL-3-mercapto-2-benzylpropanoyl)-glycine) is a small bioactive molecule, which was first introduced in 1980 [8] and currently has many possible applications in medicine [9,10]. In spite of its practical importance, thiorphan adsorption on surfaces was studied only recently [11]. By using AFM thiorphan adsorption has been found to be guided by surface polarization of ZnO surface, which results in formation of thiorphan nanodots on polar ZnO surfaces and nanoislands on nonpolar ZnO surfaces [11]. These high-resolution AFM data were corroborated experimentally by angle resolved X-ray photoelectron spectroscopy and theoretically by force field molecular dynamics and density functional tight binding simulations [11].

Prior studies showed that antibody molecular assemblies can increase secondary electron (SE) intensity [12,13] whereas bacterial clusters showed decrease in SE intensity [14]. Similarly, SE intensity was used for measuring thickness of nanometer-thin SiO_2 layers on silicon substrates [15]. However, electron emission from thiorphan structures on ZnO surfaces has not been studied yet. It is possible to obtain electron emission and topography data by AFM and SEM separately (ex-situ) using positional markers. However, preparation of such markers is not always feasible from various reasons, e.g. lithography procedures can cause substrate contamination by resist residues and subsequent plasma or chemical cleaning can cause surface modification. Moreover, structural precision of such markers to study small thiorphan nanodots should be very high (< 25 nm). Since separate measurements will be done using different scanners (i.e. AFM piezoscanner and SEM beam movement), the image alignment will also be very complicated. These are the main reasons why CPEM technique was used in this work to investigate thiorphan adsorption on different ZnO surfaces.

2. EXPERIMENTAL DETAILS

2.1 Samples preparation

Commercially available single-side polished monocrystalline 5 × 5 × 0.5 mm^3 ZnO plates from MSE supplies (USA) were used: polar Zn-face (0001), polar O-face $(000\bar{1})$, nonpolar $(10\bar{1}0)$, and nonpolar $(11\bar{2}0)$ samples. Samples were cleaned with ethanol and DI water using cotton buds before thiorphan adsorption to remove possible contaminations. Thiorphan (Alchemica s.r.o.) was dissolved in ethanol to concentration 1 mg/mL. Each sample was placed into eppendorf tube cover, placed upside-down. 200 µL of thiorphan in ethanol solution was added to each cover and eppendorf tube was closed. After 48 h deposition the ZnO samples were rinsed with ethanol, DI water and dried with nitrogen [11].

2.2 AFM-in-SEM measurements and correlation

SEM measurements were performed in EVO 10 SEM using 10 kV accelerating voltage and 100 pA current. SEM can image much larger areas than available for AFM scanner (65 × 65 μm^2), thus allow getting information from larger areas. As ZnO samples were undoped, samples were prone to charging during SEM measurements. Some areas, which were brighter than background, in some cases became darker than background after long SEM measurements. Common conductive sample coating was not used in order to study directly the electron emission properties of thiorphan. SEM images obtained by EVO 10 software with standard parameters had low contrast on all samples. Therefore, all secondary electron intensity (SE) images, presented in **Figure 1**, were obtained with specifically selected brightness and contrast separately for each image in order to increase the contrast and signal-to-noise ratio. All backscattered electron intensity (BSE) images, presented in **Figure 1**, were obtained at highest recommended brightness and contrast (50% and 80% respectively) in the high gain regime. Moreover, those images were obtained at low 1024 × 768 px^2 resolution and relatively high accumulation time at each pixel (0.1 ms) in order to improve the contrast. Additional 1 px blur and auto brightness were applied to those images using Photoshop in order to improve image visibility.

SE and BSE data, presented in the **Figures 2 and 3** and used for CPEM correlation analysis, were acquired during AFM-in-SEM data acquisition simultaneously with AFM topography data by LiteScope controller. For those measurements 20 kx SEM magnification in the spot mode was used in order to make the SEM beam spot size as small as possible. Such data collection at 650 × 650 px^2 resolution is limiting the accumulation time to 5 min; therefore, such SEM data used for CPEM correlation could be noisier than in the standard SEM regime.

AFM measurements were performed in the CPEM regime using LiteScope AFM placed in the EVO 10 SEM chamber. Self-sensing Akiyama cantilevers with nominal stiffness 5 N/m were used for the measurements. Absence of laser makes the LiteScope AFM sufficiently small, that it can fit into practically every SEM chamber

[7]. Unfortunately, usage of self-sensing cantilevers is also limiting the maximum resolution. For example, nominal tip radius of Akiyama cantilevers NV-A-Probe (Nanosensors) is 15 nm and currently no ultrasharp self-sensing cantilevers (tip radius 1 nm) are available. AFM topography, frequency shift and amplitude of cantilever oscillations images were collected by LiteScope software from 13 × 13 μm^2 area at 650 × 650 px^2 resolution in semi-contact mode with setpoint 10 - 15 Hz, scanning speed 5 µm/s and feedback settings CI = 0.05 - 0.2, CP = 0.2-0.3. The offset between SEM beam and AFM probe was around 1 µm. Its change was negligible during 1 h image acquisition.

Presented 2D AFM topography, SE, BSE and 3D CPEM images were made using Gwyddion software [16]. The alignment of simultaneously obtained AFM and SEM images and CPEM correlation analysis was performed using Matlab software. The thiorphan nanodots size is ~ 25 nm; therefore, the image alignment has to be done with very high precision. Since the AFM and SEM data were obtained using the same scanner in CPEM and the change of the offset between AFM tip and SEM beam was negligible, only X/Y changes in offset were optimized with < 25 nm precision using method similar to the least square method. In case of independently obtained images on AFM and SEM, the optimization of the relative image rotation, drift and scan size calibration would also be required, which will make reliable correlation at such high precision much more complicated if not impossible.

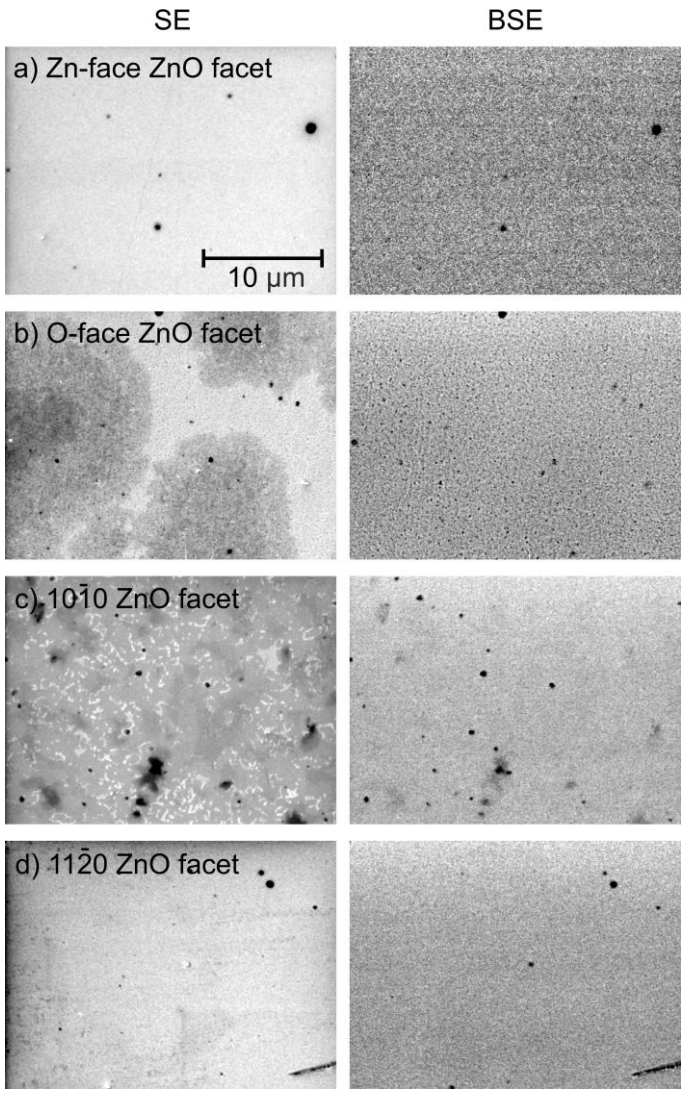

Figure 1 SE and BSE images of the thiorphan structures adsorbed on the a) Zn-face ZnO surface, b) O-face ZnO surface, c) $(10\bar{1}0)$ ZnO surface; d) $(11\bar{2}0)$ ZnO surface.

3. RESULTS

Figure 1 shows secondary electron intensity (SE) and backscattered electron intensity (BSE) images of the thiorphan structures adsorbed on the different ZnO surfaces. SEM revealed some inhomogeneity across the samples. The most representative areas are shown here. Thiorphan assembly on the polar Zn-face ZnO surface results in formation of small (4 nm) nanodots [11]. Such small objects should not be detectable by SEM. **Figure 1a** shows that indeed no fine features can be seen by SEM on the Zn-face ZnO surface.

Thiorphan assembly on the polar O-face ZnO surface results in formation of larger (25 nm) nanodots [11]. Such objects should be resolvable by SEM. **Figure 1b** shows that indeed thiorphan nanodots can be seen by SEM on the O-face ZnO surface. Nanodots form also larger scale assemblies (autocorrelation length Lx ~ 5 μm) with different electron emission properties.

Thiorphan assembly on the nonpolar $(10\bar{1}0)$ and $(11\bar{2}0)$ ZnO surfaces result in formation of 4 nm thick layers which can also form multilayer nanoislands [11]. Such multilayered objects should be detectable by SEM. **Figure 1c** shows that thiorphan multilayer nanoislands can be resolved by SEM on the nonpolar $(10\bar{1}0)$ ZnO surface. **Figure 1d** shows that few layers thiorphan nanoislands can also be seen, albeit barely, on the nonpolar $(11\bar{2}0)$ ZnO surface. The reason is probably smaller amount of tall thiorphan structures compared to the nonpolar $(10\bar{1}0)$ ZnO surface. The polar O-face ZnO and the nonpolar $(10\bar{1}0)$ ZnO samples were thus used as the most suitable and interesting objects for correlative study by the CPEM measurement and analysis.

3.1 Thiorphan assembly on the polar O-face ZnO surface

Figures 2a-c show simultaneously measured detailed AFM topography, SE and BSE intensity images, obtained on the thiorphan structures on the polar O-face ZnO surface. Individual 25 – 30 nm tall thiorphan spherical assemblies are clearly distinguishable in topo, SE and BSE images. Thiorphan spheres have clearly higher SE and BSE signal than the underlying ZnO substrate. BSE image is very similar to SE image, yet is seems a bit sharper and with higher contrast. **Figure 2d** shows 3D CPEM image, on which surface topography is presented as 3D morphology, while SE intensity is mapped over it as a blue-cyan gradient correspondingly to SE intensity. Background ZnO surface is darker than the thiorphan spheres. **Figure 2e** shows the model of thiorphan adsorption on the polar O-face ZnO surface and the direction of electric field created by ZnO surface dipole. **Figure 2f** shows correlation between the SE/BSE intensity and the thiorphan structure height on the polar surface. CPEM images contain ~ 350.000 AFM height / SE (or BSE) intensity data points each, 99.9 % of them are concentrated in a continuous black area and only 0.1% of them are visible as separate black dots. The data correlation was evaluated by the linear regression. The black dot outliers, which are located in high AFM height region above or below the linear fit, are due to the presence of 1-2 tall objects. They were included in the linear fitting, but their weight is negligible (<0.1%), thus the linear trend line is not noticeably affected. The linear regression fit (red line) clearly shows that the higher the structure, the higher the SE/BSE intensity. Such dependence is similar to antibodies [12,13], but opposite to bacteria [14].

3.2 Thiorphan assembly on the nonpolar $(10\bar{1}0)$ ZnO surface

Figures 3a-c show simultaneously measured AFM topography, SE and BSE intensity images, obtained on the thiorphan structures on the nonpolar $(10\bar{1}0)$ ZnO surface. Thiorphan assemblies have lower SE and BSE signal than underlying ZnO substrate. BSE image is very similar to SE image, yet is seems less noisy and with higher contrast, individual thiorphan layers are also better visible. **Figure 3d** shows 3D CPEM image, on which surface topography is presented as 3D morphology, while SE intensity is mapped over it as a blue-cyan gradient correspondingly to SE intensity. **Figure 3e** shows the model of thiorphan adsorption on O-face ZnO surface and the direction of electric field created by ZnO surface dipole. **Figure 3f** shows the correlation between the SE/BSE intensity and the thiorphan structure height on the non-polar surface. The data outliers

are again due to the presence of few tall objects. They were included in the linear fitting, but their weight is negligible (<0.1%), thus the linear trend line is not noticeably affected. The linear fit shows that there is a clear anti-correlation between the SE intensity and the thiorphan structure height: the higher the structure, the lower the SE intensity. This is opposite to the observation on the polar ZnO surface (**Figure 2**). Such dependence is similar to bacteria [14], but it is opposite to antibodies [12,13].

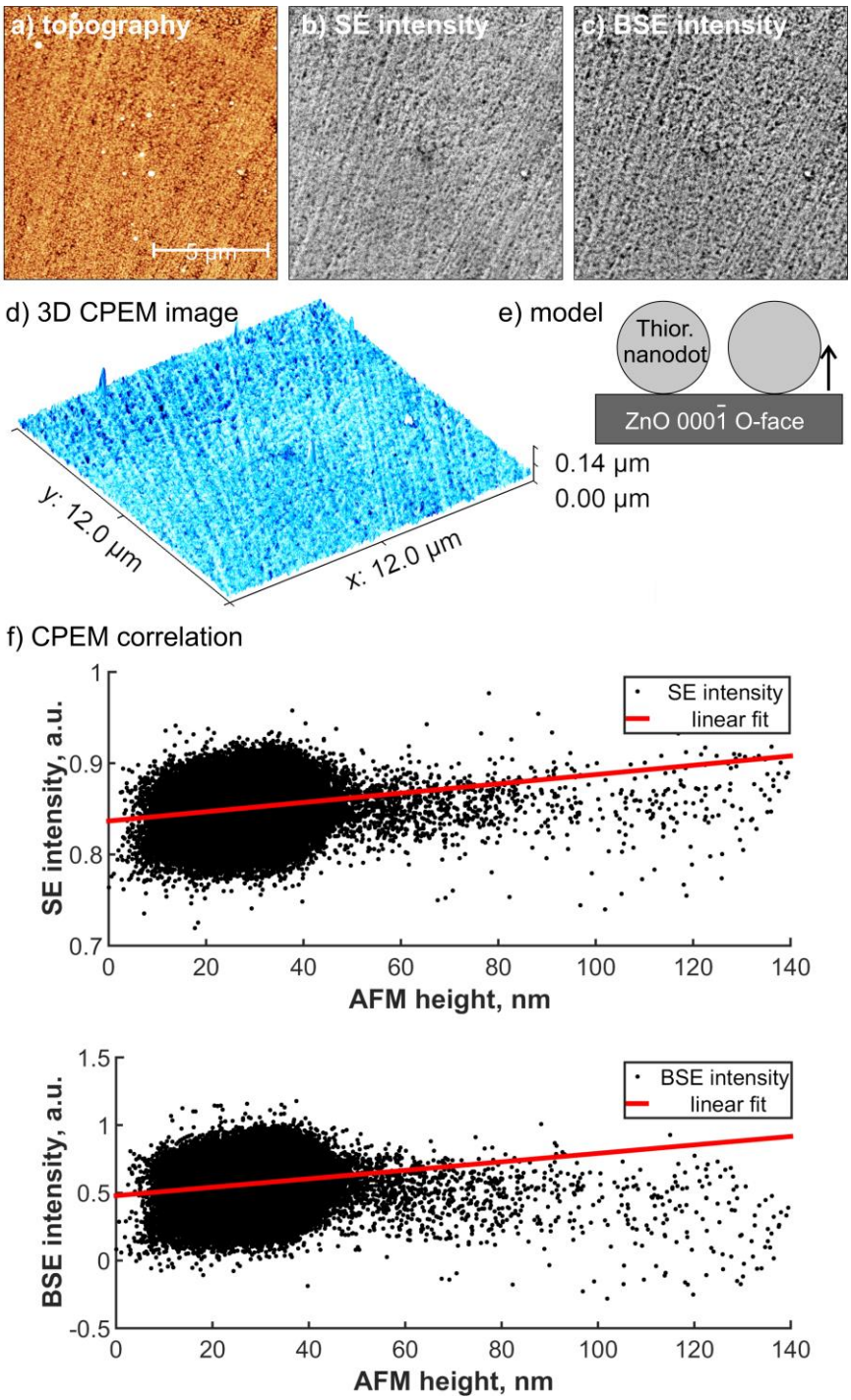

Figure 2 a) AFM, b) SE and c) BSE images of the thiorphan structures on the polar O-face ZnO surface; d) 3D CPEM image of the thiorphan structures on the O-face ZnO surface; e) the model of thiorphan assembled structures and direction of ZnO surface dipole shown by the arrow; f) CPEM correlation between SE/BSE intensity and AFM height.

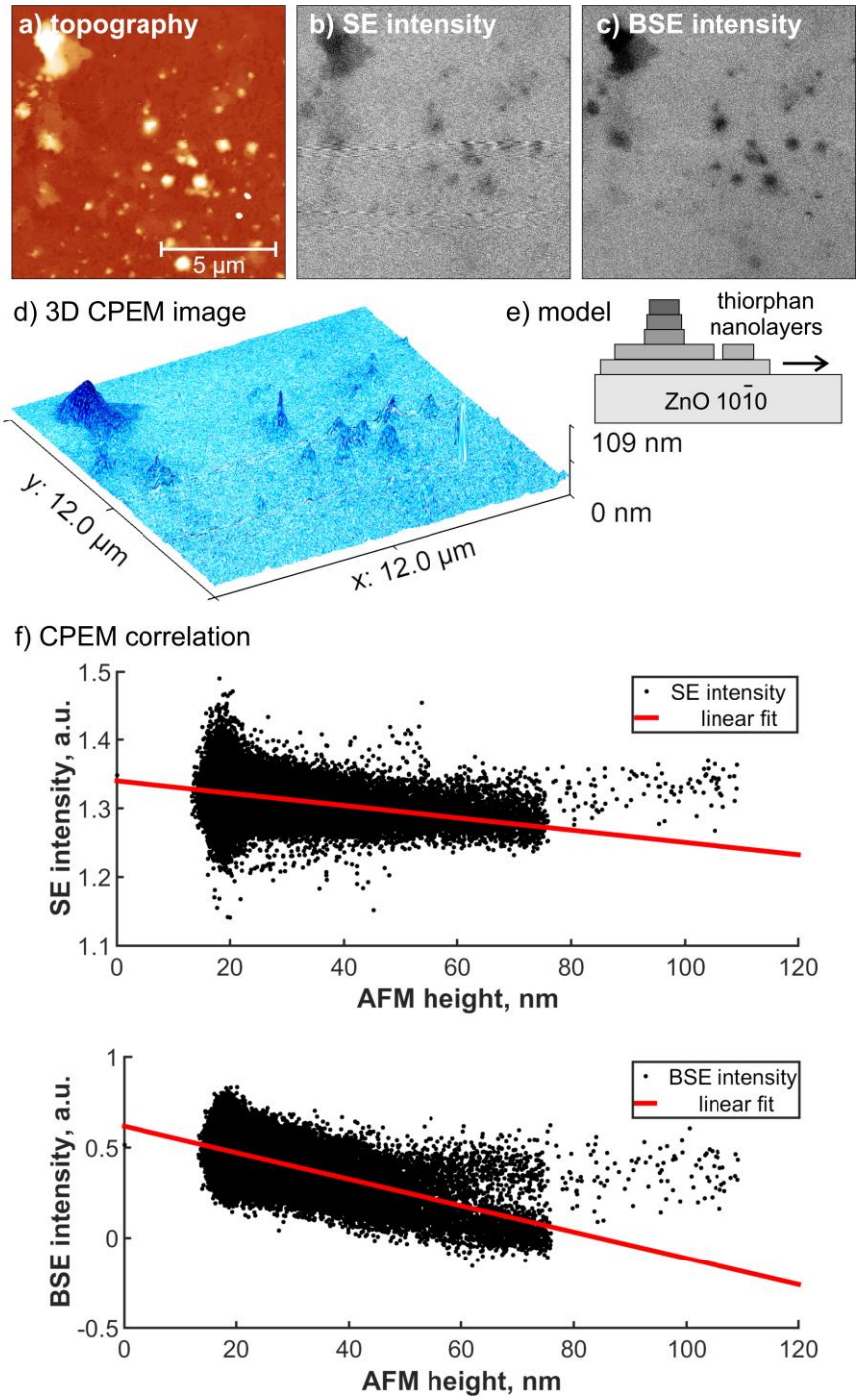

Figure 3 a) AFM, b) SE and c) BSE images of the thiorphan structures on the nonpolar $(10\bar{1}0)$ ZnO surface; d) 3D CPEM image of the thiorphan structures on the $(10\bar{1}0)$ ZnO surface; e) the model of thiorphan assembled structures and direction of ZnO surface dipole shown by the arrow; f) CPEM correlation between SE/BSE intensity and AFM height.

4. DISCUSSION

Our results show that depending on the surface polarity dipole orientation of the ZnO surface, tall thiorphan structures may have either higher (on the polar O-face ZnO surface) or lower (on the nonpolar the $(10\bar{1}0)$ surface) SE/BSE intensity. In other words, same material on the substrates with same composition results in

different SE/BSE contrast. One possible reason is the formation of different thiorphan structures on different ZnO surfaces, which is due to different interaction between thiorphan molecules and Zn/O atoms from ZnO substrate and different interaction between thiorphan molecules and surface dipoles of ZnO surfaces [11].

From electron microscopy point of view, the difference in secondary electron intensity can be mainly by three factors: different efficiency of their excitation in the material, different surface structure and chemistry, and different shading from surface layers. The material chemical composition is the same. Penetration depth of 10 keV electron beam is few microns for thiorphan molecules made from C, O, N, S and H atoms [14]. Thus, flat thiorphan layers on the nonpolar $(10\bar{1}0)$ surface in order to be darker than ZnO background have to shade secondary electrons, as in the case of bacteria [14]. However, the spherical thiorphan particles on the polar O-face ZnO surface in order to be brighter than ZnO background have to actually emit (or reflect) electrons themselves. This explanation is corroborated by the clear fine structure of the SE and BSE images on the polar surface (**Figure 2**) and dark features in both SE and BSE images on the non-polar surface (**Figure 3**).

5. CONCLUSIONS

In this work the thiorphan assembly on different ZnO surfaces was studied by CPEM (AFM-in-SEM). Correlative AFM-in-SEM data from the same region of interest were obtained under the same conditions simultaneously. The data reveal that depending on surface polarity dipole orientation, thiorphan molecular structures may have either higher (on the polar O-face ZnO surface) or lower (on the nonpolar $(10\bar{1}0)$ surface) SE/BSE intensity. The effect has been attributed to secondary electron emission in the first case and electron shading mechanism in the latter case. Such direct height/SE correlation on nanoscale features would be hard to get by individual AFM and SEM imaging. The results also hint at possibly a more general effect where the same material (molecular or other) in differently assembled structures (that can be controlled by substrate dipoles or electric field in general) can result in opposite SE and BSE contrast on the same substrate material.

ACKNOWLEDGEMENTS

This work has been supported by the project TM03000033 (TAČR).

REFERENCES

[1] CAPLAN, J.; NIETHAMMER, M.; TAYLOR, R. M. and CZYMMEK, K. J. The power of correlative microscopy: multi-modal, multi-scale, multi-dimensional. *Curr. Opin. Struct. Biol*. 2021, vol. 21, pp. 686–93.

[2] VAN RIJNSOEVER, C.; OORSCHOT, V. and KLUMPERMAN, J. Correlative light-electron microscopy (CLEM) combining live-cell imaging and immunolabeling of ultrathin cryosections. *Nat. Methods.* 2008, vol. 5, pp. 973–80.

[3] GEISSE, N. A. AFM and combined optical techniques. *Mater. Today.* 2009, vol. 12, pp. 40–5.

[4] LIU, M.; LI, Q.; LIANG, L.; LI, J.; WANG, K.; LI, J.; LV, M.; CHEN, N.; SONG, H.; LEE, J.; SHI, J.; WANG, L.; LAL, R. and FAN, C. Real-time visualization of clustering and intracellular transport of gold nanoparticles by correlative imaging. *Nat. Commun*. 2017, vol. 8, pp. 15646.

[5] ZIESCHE, R. F.; ARLT, T.; FINEGAN, D. P.; HEENAN, T. M. M.; TENGATTINI, A.; BAUM, D.; KARDJILOV, N.; MARKÖTTER, H.; MANKE, I.; KOCKELMANN, W.; BRETT, D. J. L. and SHEARING, P. R. 4D imaging of lithium-batteries using correlative neutron and X-ray tomography with a virtual unrolling technique. *Nat. Commun*. 2020, vol. 11, pp. 777.

[6] NEUMAN, J.; NOVACEK, Z.; PAVERA, M. and NOVOTNA, V. Correlative Probe and Electron Microscopy CPEM™ – The Novel Technology for 3D Material Surface Analysis. *Microsc. Microanal*. 2019, vol. 25, pp. 430–1.

[7] NEUMAN, J.; NOVAČEK, Z.; NOVOTNÁ, V.; HEGROVÁ, V. and FLAJSMAN, L. (2020). LITESCOPE™ AFM-In-Sem: Advanced Tool for Correlative Imaging and Surface Characterization. In NANOCON 2019, pp. 568–72. Available from: https://doi.org/10.37904/nanocon.2019.8655.

[8] ROQUES, B. P.; FOURNIÉ-ZALUSKI, M. C.; SOROCA, E.; LECOMTE, J. M.; MALFROY, B.; LLORENS, C. and SCHWARTZ, J. C. The enkephalinase inhibitor thiorphan shows antinociceptive activity in mice. *Nature.* 1980, vol. 288, pp. 286–8.

[9] TEJEDOR-REAL, P.; MICO, J. A.; MALDONADO, R.; ROQUES, B. P. and GIBERT-RAHOLA, J. Implication of endogenous opioid system in the learned helplessness model of depression. *Pharmacol. Biochem. Behav*. 1995, vol. 52, pp. 145–52.

[10] YANG, X.; ROJANASAKUL, Y.; WANG, L.; MA, J. Y. C. and MA, J. K. H. Enzymatic degradation of luteinizing hormone releasing hormone (LHRH)/[D-Ala6]-LHRH in lung pneumocytes. *Pharm. Res*. 1998, vol. 15, pp. 1480-4.

[11] UKRAINTSEV, E.; HEMATIAN, H. and REZEK, B. Polarization Controlled Assembly of Ultrathin Thiorphan Nanostructures on ZnO Surface Surfaces*. Langmuir.* 2023, vol. 39, pp. 1764–74. Available from: https://doi.org/10.1021/acs.langmuir.2c02393.

[12] OGURA, T. High-Contrast Observation of Unstained Proteins and Viruses by Scanning Electron Microscopy. J. Qiu, ed*. PLoS ONE.* 2012, vol. 7, e46904.

[13] ZHANG, Q.; ZHANG, M.; DU, Y.; XU, B.; CHEN, G.; HE, S.; ZHANG, D.; LI, Q. and WANG, H.-X. Trace detection of SARS-CoV-2 N-protein by diamond solution-gate field-effect transistor. *Diam. Relat. Mater*. 2023, vol. 134, pp. 109775.

[14] RUTHERFORD, D.; KOLAROVA, K.; CECH, J.; HAUSILD, P.; KULICEK, J.; UKRAINTSEV, E.; STEHLIK, S.; DAO, R.; NEUMAN, J.; REZEK, B. Correlative Atomic Force Microscopy and Scanning Electron Microscopy of Bacteria-Diamond-Metal Nanocomposites. *Ultramicroscopy.* 2024, vol. 258, pp. 113909. Available from: https://doi.org/10.1016/j.ultramic.2023.113909.

[15] KITA, Y.; KASAI, Y.; HASHIMOTO, S.; IIYAMA, K. and TAKAMIYA, S. Application of Brightness of Scanning Electron Microscope Images to Measuring Thickness of Nanometer-Thin SiO_2 Layers on Si Substrates*. Jpn. J. Appl. Phys*. 2001, vol. 40, pp. 5861.

[16] Available from: http://gwyddion.net/.